PROTEINS
STRUCTURE ■ FUNCTION ■ BIOINFORMATICS

Structural insights into the stabilization of active, tetrameric DszC by its C-terminus

Liang Zhang,[1] Xiaolu Duan,[1] Daming Zhou,[1] Zhe Dong,[1] Kaihua Ji,[1] Wuyi Meng,[2] Guoqiang Li,[1]* Xin Li,[1]* Haitao Yang,[3] Ting Ma,[1] and Zihe Rao[1]

[1] College of Life Sciences, Nankai University, Tianjin, China

[2] Elias James Corey Institute of Biomedical Research, Jiangyin, Jiangsu, China

[3] School of Life Sciences, Tianjin University, Tianjin, China

ABSTRACT

Dibenzothiophene (DBT) is a typical sulfur-containing compound found in fossil fuels. This compound and its derivatives are resistant to the hydrodesulfurization method often used in industry, but they are susceptible to enzymatic desulfurization via the 4S pathway, which is a well-studied biochemical pathway consisting of four enzymes. DBT monooxygenase (DszC) from *Rhodococcus erythropolis* is involved in the first step of the 4S pathway. We determined the crystal structure of DszC, which reveals that, in contrast to several homologous proteins, the C-terminus (410–417) of DszC participates in the stabilization of the substrate-binding pocket. Analytical ultracentrifugation analysis and enzymatic assays confirmed that the C-terminus is important for the stabilization of the active conformation of the substrate-binding pocket and the tetrameric state. Therefore, the C-terminus of DszC plays a significant role in the catalytic activity of this enzyme.

Proteins 2014; 82:2733–2743.

Key words: crystal structure; enzyme mechanism; C-terminus; monooxygenase; tetramerization.

INTRODUCTION

With increasing petroleum consumption, particularly that of high-sulfur crude oil, air pollution due to oxysulfides represents a serious concern.[1] The polycyclic aromatic sulfur heterocyclic (PASH) compound dibenzothiophene (DBT) and its derivatives are typical sulfur-containing compounds found in fossil fuels.[2] Because DBT is resistant to hydrodesulfurization,[3,4] an alternative pathway, enzymatic desulfurization, is more favorable. The 4S pathway is a classical and well-studied DBT desulfurization pathway that employs two classes of enzymes: flavin-dependent monooxygenases, which include DszA and DszC, and the desulfinase DszB. In this pathway, DszC oxidizes DBT first to dibenzothiophene sulfoxide (DBTO) and, subsequently, to dibenzothiophene sulfone ($DBTO_2$). DszA then further oxidizes $DBTO_2$ to 2-hydroxybiphenyl-2-sulfinic acid (HBPS). Finally, DszB hydrolyzes HBPS into 2-hydroxybiphenyl (HBP) and sulfite. Additionally, the flavin mononucleotide NADH reductase (DszD) also plays important roles during the first three enzymatic steps (Fig. 1).[4–10] However, as DszC oxidizes DBT early in this process, it is the most important enzyme in the 4S pathway.

DszC from *Rhodococcus erythropolis*, which uses the reduced form of FMN as its cofactor, consists of 417 residues and forms a tetramer in solution.[11] To date, more than ten similar oxidoreductase structures have been reported. Interestingly, for some of these oxidoreductases, conformational changes at the C-terminus have been

Additional Supporting Information may be found in the online version of this article.

Abbreviations: AUC, analytical ultracentrifugation; DBT, dibenzothiophene; DBTO, dibenzothiophene sulfoxide; DBTO2, dibenzothiophene sulfone; DszC, DBT monooxygenase; FMN, flavin mononucleotide; HBP, 2-hydroxybiphenyl; HBPS, 2-hydroxybiphenyl-2-sulfinic acid; PASH, polycyclic aromatic sulfur heterocyclic.

Grant sponsor: National Key Basic Research Program of China (973 Program); Grant number: 2014CB542800, 2010CB833600; Grant sponsor: Young Scientists Fund of the National Natural Science Foundation of China; Grant numbers: 31000345, 31000056; Grant sponsor: Funds for National Basic Science Personnel Training; Grant number: J1103503; Grant sponsor: Natural Science Foundation of Tianjin, China; Grant number: 09JCZDJC18000; Grant sponsor: The Fundamental Research Funds for the Central Universities.

Liang Zhang and Xiaolu Duan contributed equally to this work.

*Correspondence to: Guoqiang Li, College of Life Sciences, Nankai University, Tianjin, China. E-mail: gqli@nankai.edu.cn or Xin Li, College of Life Sciences, Nankai University, Tianjin, China. E-mail: lix1980@nankai.edu.cn

Received 27 January 2014; Revised 2 June 2014; Accepted 18 June 2014
Published online 28 June 2014 in Wiley Online Library (wileyonlinelibrary.com).
DOI: 10.1002/prot.24638

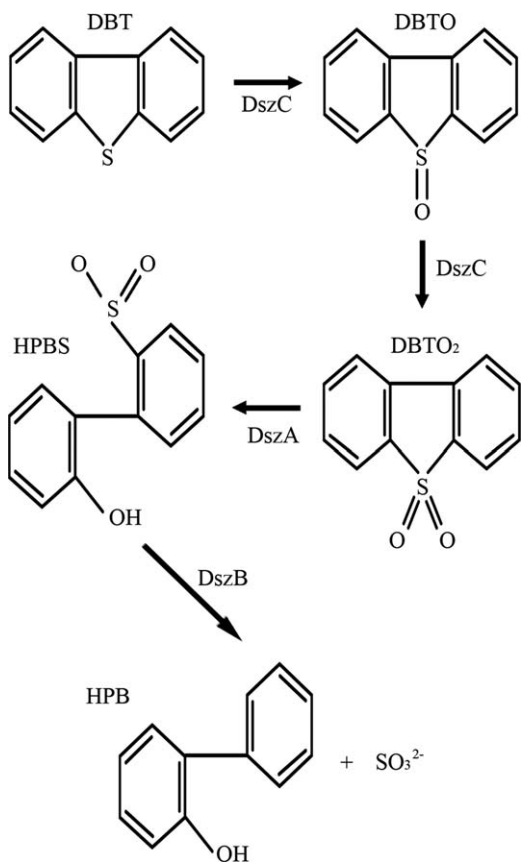

Figure 1

A brief overview of the 4S pathway used for biodesulfurization of DBT by *R. erythropolis* DS-3. DszC successively oxidizes DBT to DBTO and $DBTO_2$. Subsequently, the $DBTO_2$ monooxygenase (DszA) catalyzes the transformation of $DBTO_2$ into HBPS. Finally, the HBPS desulfinase (DszB) hydrolyzes HBPS to HBP and sulfite.

associated with coenzyme binding[12,13] or enzyme oligomerization.[14]

We have crystallized DszC from *Rhodococcus erythropolis* previously.[15] In this study, we found that the DszC C-terminus, which is located in the interior of the protein, plays a crucial role in tetramerization and in the formation of the substrate-binding pocket. Therefore, we conclude that the C-terminus is critical for DszC activity.

MATERIALS AND METHODS

Crystallization

Wild-type DszC was expressed and purified as previously described.[15] The protein was expressed in *E. coli* BL21(DE3) cells transformed with a pET-28a plasmid containing the *dszC* gene. The recombinant protein containing an N-terminal His-tag was purified using sequential nickel-affinity, anion-exchange and size-exclusion chromatography. The purified DszC protein was mixed with FMN at a 1:10 molar ratio in a solution containing 20 m*M* Tris-HCl (pH 8.0) and 150 m*M* NaCl. The final concentration of the DszC protein in the mixture was 20 mg mL^{-1}. After an overnight incubation at 277 K, the mixture was used for crystallization via the hanging drop vapor diffusion method. Two microliters of the DszC-FMN solution was mixed with 2 μL of a reservoir solution [200 m*M* lithium sulfate, 100 m*M* Bis-Tris (pH 6.5) and 35% (w/v) polyethylene glycol (PEG) 3350] prior to equilibration against 300 μL of reservoir solution. After ~1 week, large yellow plate crystals (~0.3 mm × 0.2 mm × 0.05 mm) were collected for diffraction experiments.

Data collection and structure refinement

Diffraction data were collected using an in-house X-ray source system (generator: Rigaku, MicroMax-007HF, College of Life Science, Nankai University, P.R. China; detector: R-AXIS HTC; X-rays: Cu Kα) at ~100 K. The dataset was processed using the XDS package,[16] HKL2000,[17] and CCP4 suite[18] software programs. The DszC structure was determined by molecular replacement using PHASER[19] and our previously reported[15] DszC structure (PDB code: 4JEK) as the search model. The structure was refined using REFMAC5,[20] PHENIX,[21] and Coot.[22] The structure of the final model was verified using MolProbity.[23] All structural figures were rendered using PyMOL.[24]

Mutant construction

The DszC mutants were constructed using an overlapping polymerase chain reaction (PCR) technique[25] and *Pfu* DNA polymerase (Thermo Fisher Scientific). The resultant PCR product was ligated into the pET-28a(+) vector (Novagen) for subsequent sequence analysis. Subsequently, the verified recombinant plasmids were transformed into *E. coli* BL21(DE3) competent cells (Novagen) for protein expression, and the mutant proteins were purified as described for the wild-type DszC protein.[15]

Analytical ultracentrifugation

Analytical ultracentrifugation (AUC) was performed using a Beckman Coulter XL-I analytical ultracentrifuge with six-channel centerpieces and sapphirine windows at 42,000 rpm and 277 K with absorbance detection.[26] For the assay, we used a purified protein solution (400 μL; 1 mg mL^{-1}) in loading buffer containing 20 m*M* Tris-HCl (pH 8.0) and 150 m*M* NaCl. The data were analyzed using the SEDFIT and SEDPHAT software programs.[27,28] Neither substrate nor coenzyme was used in this assay.

DszC activity assay

For the activity assay, we used 1 mL of 1× phosphate-buffered saline (PBS) buffer (140 m*M* NaCl, 10 m*M*

Table I
Data Collection and Refinement

Parameter	DszC
Data collection	
Space group	$C222_1$
Cell parameters (Å, °)	$a = 130.98$, $b = 136.18$, $c = 174.83$; $\alpha = \beta = \gamma = 90$
Wavelength (Å)	1.5418
Resolution (Å)[a]	50–2.26 (2.32–2.26)
Average I/σ (I)	10.03 (1.80)
Total reflections	300,020
Unique reflections	72,630
Redundancy	4.08 (4.00)
Completeness (%)	98.8 (99.3)
R_{merge}[b]	0.115 (0.612)
Structure refinement	
Resolution (Å)	36.4–2.3
Average *B*-factor (Å^2)	35.24
R_{work}/R_{free}[c]	0.179/0.231
R.M.S.D. bond lengths (Å)[d]	0.009
R.M.S.D. bond angles (°)[d]	1.193
Number of chains	4
Number of waters	622
Ramachandran plot	
Favored (%)	98.6
Allowed (%)	1.3
Disallowed (%)	0.1[e]

[a]The numbers in parentheses correspond to the highest resolution shell.
[b]$R_{merge}=\sum_i|I_i-\langle I\rangle|/\Sigma\langle I\rangle$, where I_i is an individual intensity measurement and $\langle I\rangle$ is the average intensity for all the reflections.
[c]$R_{work}/R_{free} = \Sigma\ ||F_o|-|F_c||\ /\ \Sigma|F_o|$, where F_o and F_c are the observed and calculated structure factors, respectively.
[d]The R.M.S. deviations relate to the Engh and Huber parameters.
[e]The two Ramachandran outliers (179-Asp and 180-Asp) are localized in a loop region of chain D with poor electron density.

Na_2HPO_4, 2.7 m*M* KCl, and 1.8 m*M* KH_2PO_4) as the assay buffer supplemented with 300 μM NADH, 50 μM FMN and 50 μM DBT (a sixfold molar excess of NADH to FMN and DBT was used to ensure sufficient NADH levels). To initiate the reaction, DszC (wild type or mutant) and DszD (containing an N-terminal His-tag and expressed in *E. coli* using the purification scheme described for DszC) were both added to the assay at a final concentration of 16 μg mL^{-1} for each enzyme. During the reaction, DszD is responsible for supplying reducing equivalents in the form of $FMNH_2$ to the monooxygenase DszC.[29] The reaction was performed at 303 K for 24 h and was terminated by the addition of 1 mL of ethyl acetate to the system. With vigorous shaking, ethyl acetate was used to extract the unreacted DBT and $DBTO_2$. After the complete removal of ethyl acetate via evaporation, the substrate and product were redissolved in 1 mL of methanol and subjected to high-performance liquid chromatography (HPLC) for subsequent analysis[8,29–34]; time points during the linear portion of the reaction were used for analysis. Because residual ethyl acetate can seriously affect the accuracy of the measured product, the average substrate consumption rate from three different time points was used to determine the activity. Considering that the complex procedures used during this assay may have introduced systematic biases, we simply used "+" symbols to indicate activity rather than presenting quantitative results.

RESULTS

Structure determination

The structure of DszC was determined at 2.3-Å resolution (PDB code: 4NXL). The crystals belong to the space group $C222_1$, with 4 monomers constituting a functional tetramer per asymmetric unit. In each chain, the N-terminal residues 1–18 are disordered. As described in the Materials and Methods, we attempted to determine the DszC-FMN complex structure in this study. Additional electron density was indeed observed in each substrate-binding pocket, particularly for chain A (data not shown). However, perhaps due to low occupancy, this additional density was not fully continuous; therefore, we could not definitively attribute this density to an FMN molecule. The detailed statistics for the dataset are summarized in Table I.

Overall structure of DszC

As shown in Figure 2(A), four DszC molecules formed a regular tetrahedron. Using chain A as the model, the DszC subunit was divided into three primary sections: an N-terminal helical region (residues 19–125; α1–α6), a C-terminal helical region (residues 235–409; α7–α12) and a middle region (residues 126–234). The middle region forms a β-barrel structure (β1–β8) with helices α1–α3 and α6 located on the outside of the β-barrel; the four long bundled helices α8–α11 are nearly parallel in orientation. A substrate-binding pocket is located between the bundle and the β-barrel, and helices α4 and α5 are located behind this pocket [Fig. 2(B,C)]. In addition to the C-terminal helical region, eight additional residues (residues 410–417) were included in the C-terminus. The looped C-terminus is located inside the subunit near the substrate-binding pocket [Fig. 2(B) and Supporting Information S1].

In the tetrameric state, the buried surface area for each subunit is ~3480 Å^2. The buried surface area between chains A and D is ~1780 Å^2, which is larger than the buried surface area between chains A and C (~1450 Å^2), and the buried surface area between chains A and B is marginal and contributes only ~250 Å^2. The buried surface area is primarily composed of residues 246-Arg to 409-Gln (from α8 to α12). The C-terminal helical bundle (α8–α11) for each subunit (chain A) is nearly antiparallel to the helical bundle of one neighboring subunit (chain D) and nearly perpendicular to the helical bundle of another neighboring subunit (chain C). Helices α10 and α11 and their connecting loop form contacts with their counterparts in a neighboring subunit (chain D) in

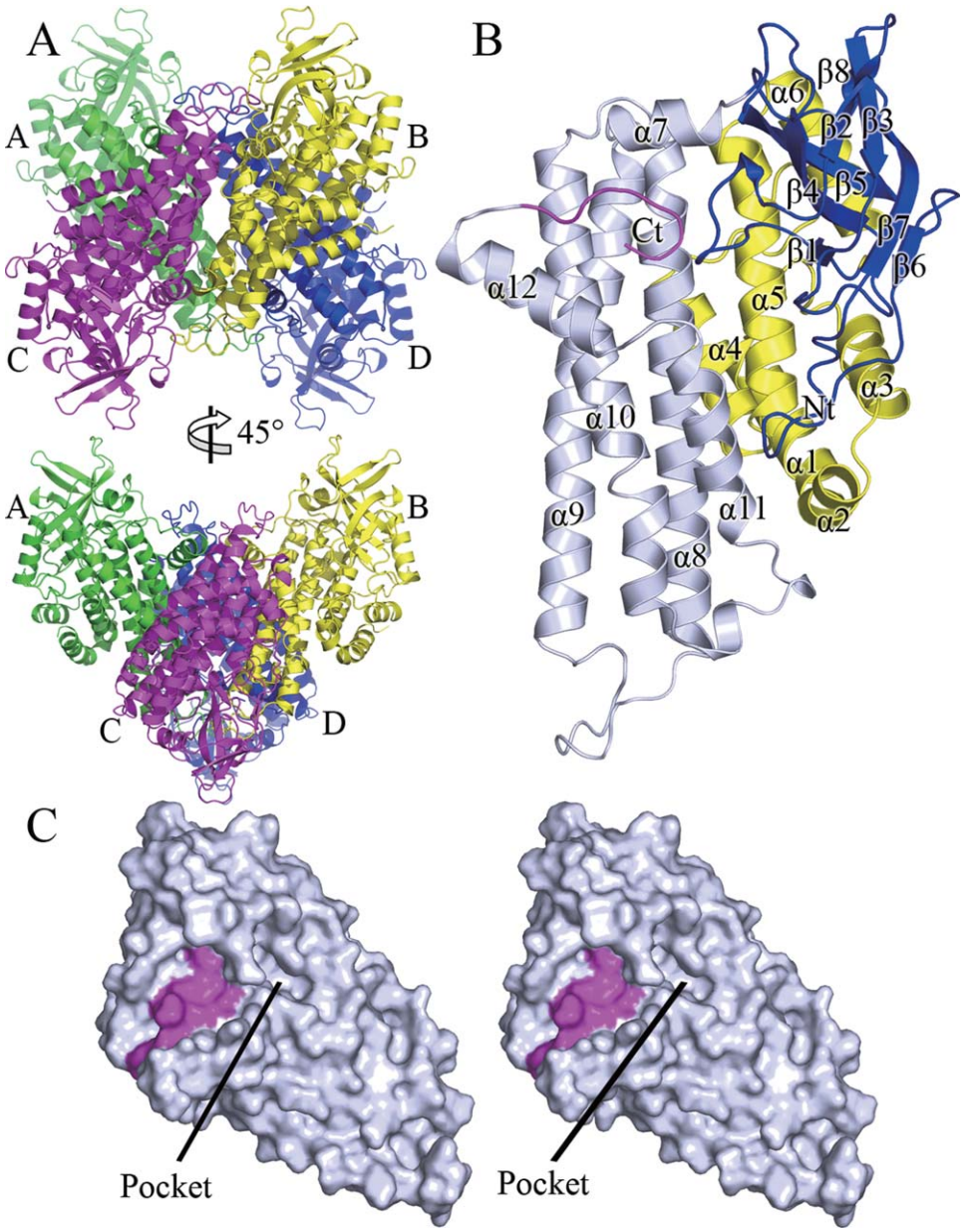

Figure 2

The overall DszC structure. (**A**) Ribbon representation of the DszC tetramer. The four subunits are colored green, yellow, magenta and blue. (**B**) Ribbon representation of the DszC subunit A. The N-terminal region (residues 19–125), the middle region (residues 126–234) and the C-terminal region (residues 235–409) are colored yellow, blue and white, respectively. The DszC C-terminus (residues 410–417) is colored magenta. (**C**) A stereoview of the DszC monomer surface. The overall surface is colored white, and the C-terminal region is colored magenta.

a nearly parallel fashion. Helix α9 of each subunit directly interacts with helices α9, α10, and α12 from a neighboring subunit (chain C) in a nearly perpendicular fashion (Supporting Information Fig. S2). We calculated that helix α12 was responsible for ~1270 $Å^2$ of the buried area in each subunit, which is more than one-third of the total buried area. Between any two neighboring subunits, helix α12 from one subunit interacts with the end of helix α9 as well as the loop region connecting helices α8 and α9 from the other subunit; in particular, this interaction localizes the 282-Arg, 284-Trp, and 370-Arg side chains close to the substrate-binding pocket of the neighboring subunit [Fig. 3(A)].

The substrate-binding pocket is composed of inner and outer chambers [Fig. 3(B)]. The inner chamber is small and composed of hydrophobic residues, including 103-Met, 174-Phe, 237-Phe, 250-Phe, 254-Ala, 258-Phe, 415-Phe, and 416-Thr (whose side-chain methyl group

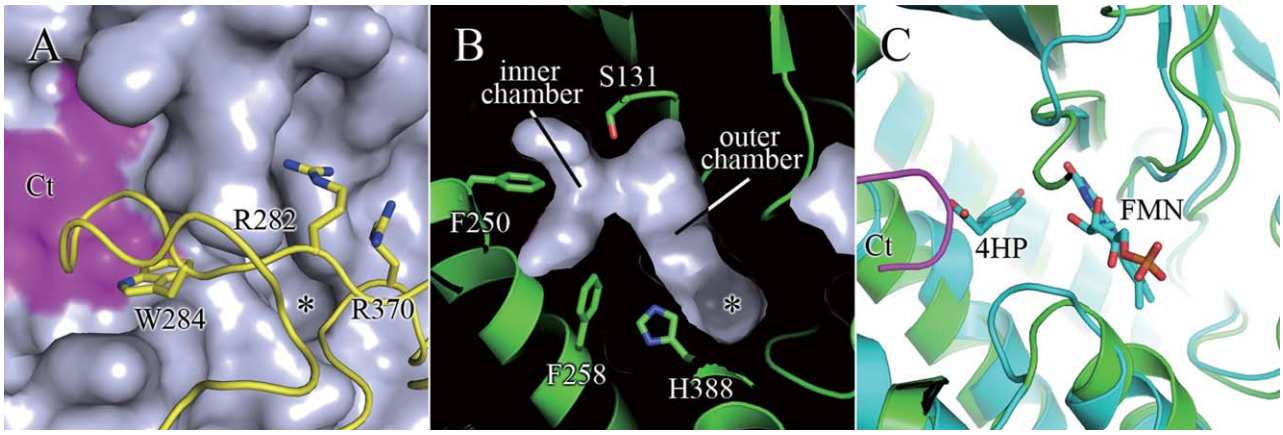

Figure 3

The substrate-binding pocket of DszC. (**A**) The entrance of the substrate-binding pocket. Chain A is presented in surface representation (colored white with magenta indicating the C-terminal region), and chain D is presented in ribbon representation (yellow) with certain residues shown as sticks. (**B**) A detailed view of the substrate-binding pocket of DszC. Chain A is shown in ribbon representation (green), and the substrate-binding pocket is shown in surface representation. The asterisk indicates identical regions of the substrate-binding pocket in panels A and B. (**C**) Comparison of the active sites of DszC (colored green with the C-terminus colored magenta) and the monooxygenase from *Acinetobacter baumannii* in complex with 4-hydroxyphenylacetate (4HP) and FMN (PDB code: 2JBT, colored cyan). The structural features of DszC in all three panels are shown in an identical orientation.

points inward towards the chamber); the side chain of 250-Phe is located at the base of the inner chamber with the other seven residues forming the periphery of the chamber from a variety of different directions. The side chains of 96-Tyr, 129-Asn, 131-Ser, 132-Ser, 134-Asn, and 391-His are distributed in a ring with their polar side chains pointing inward, narrowing the channel connecting the inner and outer chambers. The outer chamber is larger than the inner chamber and relatively flat in shape, with one side connected to the inner chamber and the other side linked to the pocket opening. Despite the narrowness of the connecting neck, the side chains of 391-His, 92-His, 163-Ser, 187-Ile, 210-Met, 388-His, and 390-Leu also contribute to form the inner surface (i.e., the side connected to the inner chamber) of the outer chamber. The residues 161-Phe, 162-Cys, 205-Trp, and 215-Ser as well as three residues (282-Arg, 369-Ala, and 370-Arg) from a neighboring subunit (chain D) compose the outer surface (i.e., the side that includes the pocket entrance) of the outer chamber. The pocket opening is hydrophilic and primarily composed of positively charged residues, including 142-Lys, 160-His and the two basic residues from chain D (282-Arg and 370-Arg). In addition, the sole acidic residue 133-Glu also helps form the pocket opening. The ellipse-shaped pocket opening is ~6 Å long and 4 Å wide.

The C-terminus (residues 410–417) is critical to DszC activity

In most structures of DszC homologs, the C-termini are disordered. Interestingly, the C-terminus (residues 410–417) of DszC is positioned in an ordered conformation in the crystal structure. 415-Phe and 416-Thr are directly involved in the formation of the hydrophobic inner chamber of the substrate-binding pocket. The main-chain carboxyl group of the last residue in the protein, 417-Ser, interacts with the side chain of 338-Arg through a salt bridge. The side-chain hydroxyl group of 417-Ser also forms a 2.5-Å hydrogen bond with the main-chain carbonyl oxygen atom of 412-Ile [Fig. 4(A)]. To elucidate the function of the C-terminus, we generated proteins with alanine substitutions at the C-terminal residues 415-Phe, 416-Thr and 417-Ser as well as at 338-Arg in helix α10, and we assayed the catalytic activities and polymeric states of these mutant proteins. As expected, both the F415A and T416A variants, which were predicted to have larger hydrophobic inner chambers in the substrate-binding pocket, showed reduced catalytic activity compared with wild-type DszC. The S417A mutation, which disrupts the hydrogen bond between 417-Ser and 412-Ile but retains the salt bridge interaction between 417-Ser and 338-Arg, negligibly influenced the catalytic activity of the enzyme (Table II). These results indicate that the hydrogen bond involving the side chain of 417-Ser has only a limited effect on catalytic activity. Analytical ultracentrifugation (AUC) assays indicated that the three mutant proteins formed stable tetramers that were similar to wild-type DszC (Fig. 5). However, the R338A mutant, which disrupts the salt bridge between 338-Arg and 417-Ser, not only impaired enzymatic activity but also affected the oligomerization state of DszC [Fig. 4(B) and Table II]. In contrast to wild-type DszC, which forms ~200-kDa tetramers,

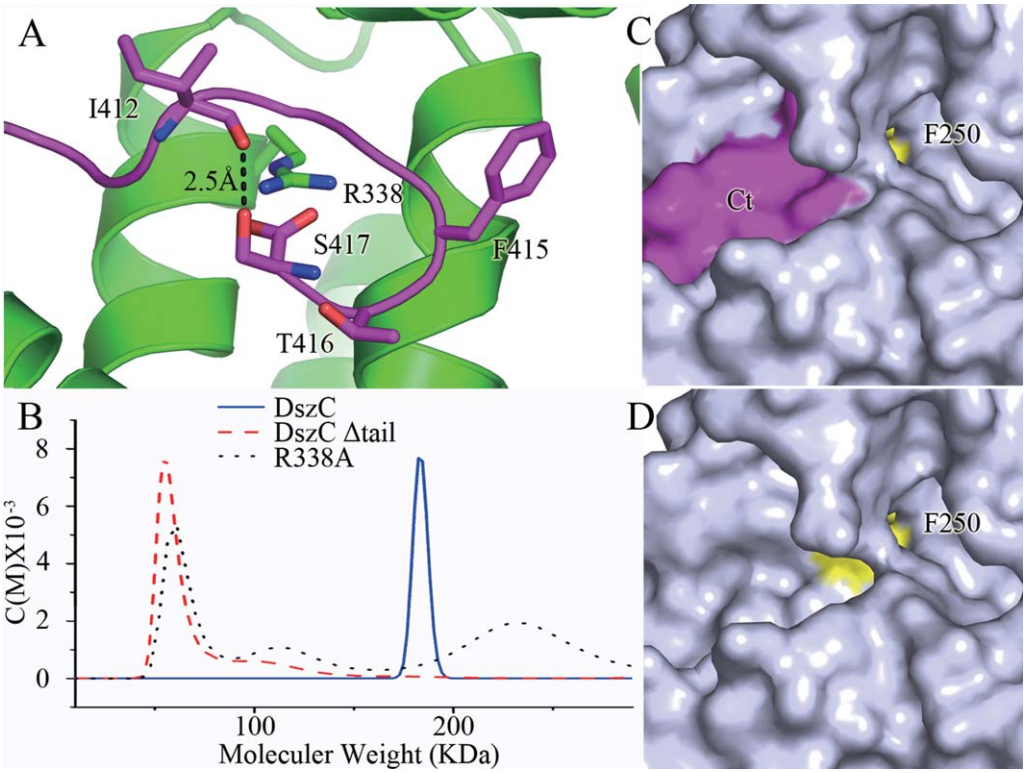

Figure 4

Details of the DszC C-terminus. (**A**) Interactions between the C-terminus and neighboring residues. The carbon atoms of the C-terminal residues (412-Leu, 415-Phe, 416-Thr, and 417-Ser) are colored magenta, and the carbon atoms of the remaining residues are colored green. Oxygen and nitrogen atoms are colored red and blue, respectively. (**B**) Analytical ultracentrifugation analysis of the wild-type and mutant DszC enzymes. The blue line indicates wild-type DszC; the red dashed line indicates the C-terminal truncation mutant; and the black dotted line indicates the R338A mutant. (**C**) and (**D**) show surface representations of the DszC substrate-binding pocket and the C-terminus. The C-terminus is colored magenta, or omitted in the case of (D), and 250-Phe is colored yellow. The structural features in panels (C) and (D) are shown in an identical orientation.

R338A predominantly formed ~50-kDa monomers in solution, along with a few other oligomerization states [Fig. 4(B)]. These results demonstrate that the ionic interaction between 338-Arg and 417-Ser is indispensable and that the C-terminus is not only linked with enzymatic activity but also influences DszC tetramer formation.

Furthermore, we truncated the last eight residues of DszC and performed activity assays on the resulting mutant protein. As observed for the R338A mutant, the truncated construct did not exhibit catalytic activity and primarily formed ~50-kDa monomers in AUC analysis [Fig. 4(B)]. This result is consistent with our hypothesis that the C-terminal residue 415-Phe plays an important role in maintaining the hydrophobic inner chamber of the substrate-binding pocket and the enzyme's activity. From the structure, we deduced that truncation of the C-terminus would expose the inner chamber of the substrate-binding pocket to solvent [Fig. 4(C,D)] and result in the collapse of the hydrophobic structure. Furthermore, because the substrate-binding pocket of the enzyme is composed of two neighboring DszC subunits, truncation of the C-terminus (which would disrupt interactions between neighboring DszC subunits) should impair formation of the substrate-binding pocket and abolish enzymatic activity, despite the overall structure of the enzyme remaining intact. In wild-type DszC tetramers, the buried area of each subunit is ~3480 Å^2, whereas truncation of the C-terminus caused a minor reduction in the buried area of each subunit to ~3430 Å^2. Therefore, we conclude that the direct effects of the C-terminus on tetramerization are negligible (~50 Å^2) and that the contributions of the C-terminus to the buried area can be largely ignored.

The residues around the substrate-binding pocket are conserved

To identify the conserved active site residues of the monooxygenase, we performed a multiple sequence alignment using the ClustalW2 program[35,36] (Fig. 6). On the basis of this alignment and our molecular structure, we determined that eight specific conserved residues (96-Tyr, 129-Asn, 161-Phe, 163-Ser, 205-Trp, 215-Ser,

Table II
Enzymatic Activity of the Various DszC Mutants[a]

Type of mutation	Result
R338A	−
S417A	++
T416A	+
F415A	+
H391A	−
Y96A	++
N129A	−
F161A	−
S163A	−
F250A	+/−
F250R	−
W205A	−
S215A	−
DszCΔtail[b]	−
DszC	+++
Control[c]	−

[a]Reactions without a detectable product (DBTO or $DBTO_2$) were considered inactive ("−"). Where products were detectable, the activities were graded based on consumption rate of the substrate DBT. For a DBT consumption rate >75%, the activity was graded as "+++"; 50–75% as "++"; 25–50% as "+"; and <25% as "+/−". The DBT consumption rate for wild-type DszC was defined as 100% and control consumption as 0%.
[b]DszCΔtail refers to the C-terminus truncation mutant.
[c]For the control group, we used the PBS buffer instead of a DszC solution.

250-Phe, and 391-His) surround and form the substrate-binding pocket, as discussed above. Each of these eight residues was individually substituted with an alanine residue, and activity assays were performed on the variants. As listed in Table II, with the exception of the Y96A mutation, seven of the mutants exhibited striking decreases in DBT monooxygenation activity, with only F250A retaining detectable catalytic activity. Although the 96-Tyr and 250-Phe side chains both help to form the hydrophobic inner chamber, the Y96A and F250A mutations did not expose the chamber to solvent, unlike the C-terminus truncation mutant; instead, the variants caused the inner chamber to enlarge, although this change did not completely impair enzymatic activity. These results are consistent with the activity assay results for F415A and T416A. Interestingly, according to the sequence alignment, 250-Phe is conserved in two of the sequences, whereas the corresponding residues in the other six sequences are arginines. To determine whether arginine can substitute for phenylalanine at this site without disturbing enzymatic activity, we created a DszC F250R mutant and assayed its activity. This mutation entirely abolished the DBT oxidation activity of the enzyme, indicating that arginine cannot be substituted for phenylalanine at this site in DszC. The side chain of arginine is longer and more hydrophilic than that of phenylalanine. Therefore, when 250-Phe is mutated to arginine, the longer arginine side chain may protrude into the inner chamber of the substrate-binding pocket and reduce the size of the chamber as well as disrupt its hydrophobicity [Fig. 3(B)]. It is possible that the diversity of amino-acid residues observed at this site in the different monooxygenases may be attributed to the distinct properties of the substrate-binding pockets, leading to differences in substrate selectivity.

DISCUSSION

To date, the structures of over ten DszC homologs have been determined. Among these, structures in complex with substrates and flavin cofactors have been reported for the *Acinetobacter baumannii* monooxygenase[37] and the *Actinomadura kijaniata* sugar N-oxygenase,[12] and the detailed catalytic mechanism has been proposed based on a structural study on the *Acinetobacter baumannii* monooxygenase. This study proposes that the enzyme first catalyzes the pre-oxidation of a reduced flavin ($FMNH_2$ or $FADH_2$), which produces a flavin C4a-hydroperoxide intermediate.[38] The intermediate then attacks the substrate and transfers an oxygen atom to the substrate. Finally, the flavin releases a water molecule, which shifts the protein to its oxidized form.

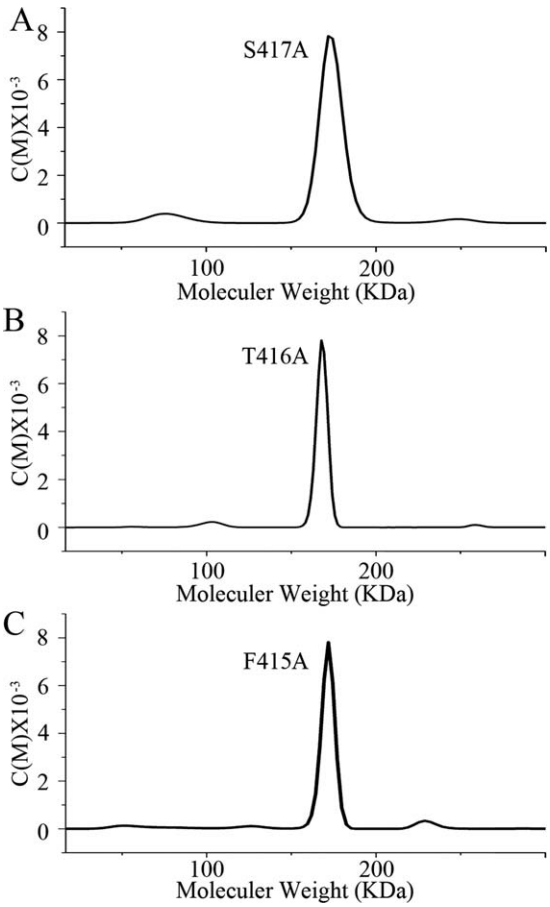

Figure 5
Analytical ultracentrifugation analysis of the three DszC mutants (**A**) S417A, (**B**) T416A, and (**C**) F415A.

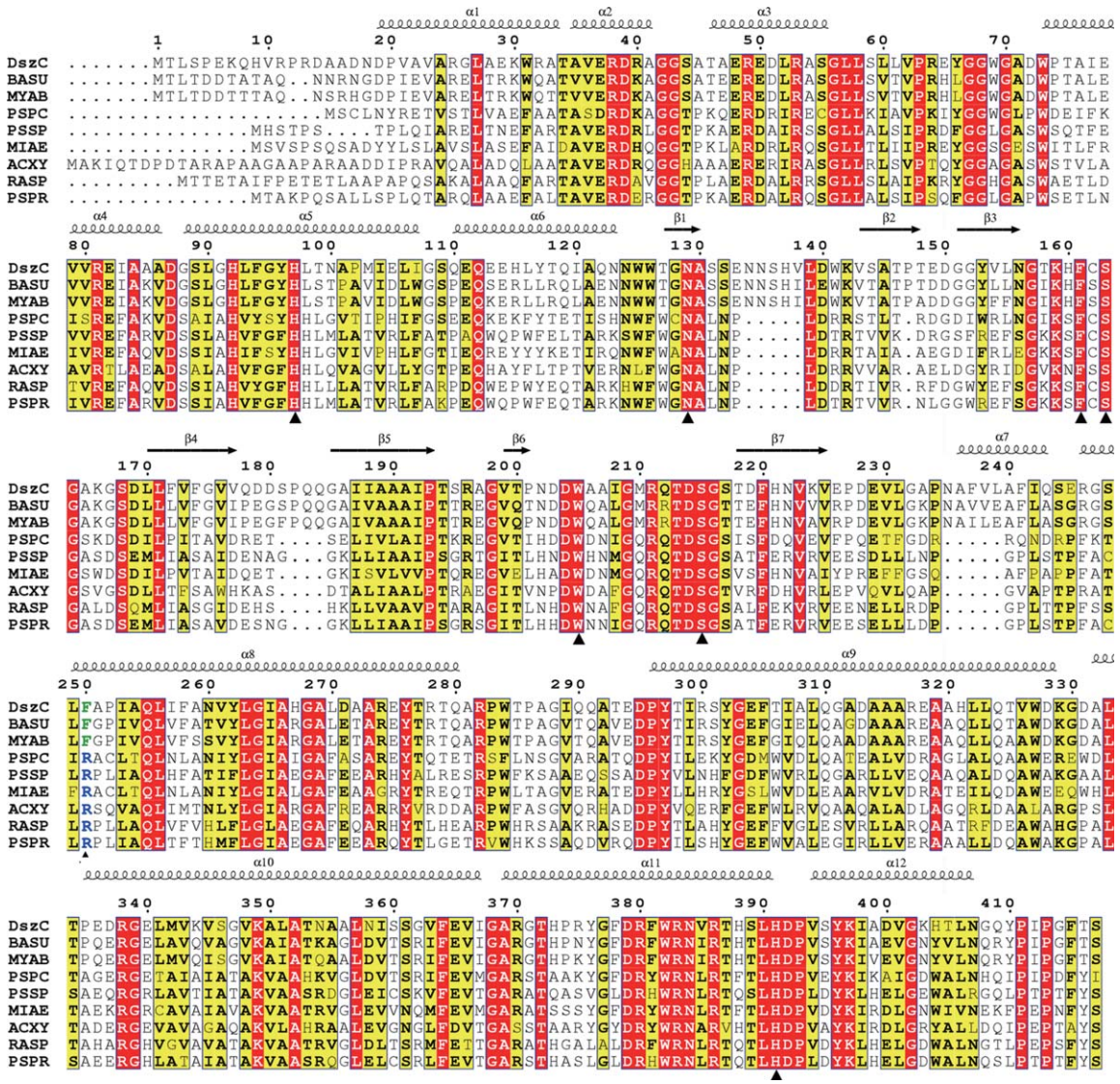

Figure 6

Multiple sequence alignment of DszC with several homologous monooxygenases. From top to bottom, the sequences represent monooxygenases from *Rhodococcus erythropolis* (denoted DszC), *Bacillus subtilis* (BASU), *Mycobacterium abscessus* 5S-0304 (MYAB), *Pseudanabaena biceps* PCC 7429 (PSPC), *Pseudomonas sp.* HYS (PSSP), *Microcystis aeruginosa* PCC 9807 (MIAE), *Achromobacter xylosoxidans* C54 (ACXY), *Ralstonia sp.5_7_47* FAA (RASP) and *Pseudomonas protegens* Pf-5 (PSPR). Identical residues are highlighted with a red background, and conserved residues are shown in bold with a yellow background. The conserved active site residues are indicated with black triangles. The phenylalanine or arginine residues corresponding to 250-Phe in wild-type DszC are indicated by a green "F" or a blue "R", respectively.

Considering the structural similarities between DszC and the monooxygenase from *Acinetobacter baumannii* [Fig. 3(C)], these two enzymes should share an identical catalytic mechanism, which is also utilized by the sugar N-oxygenase from *Actinomadura kijaniata*.

Based on previous studies, the C-terminus of the sugar N-oxygenase from *Actinomadura kijaniata* is disordered when not bound to a flavin molecule.[13] However, upon substrate and cofactor binding, the C-terminus is thought to become ordered and to interact with residues near the active site.[12] These observations suggest that the C-terminus of the sugar N-oxygenase from *Actinomadura kijaniata* is involved in substrate and coenzyme binding and release. In contrast, the DszC C-terminus is thought to form an ordered substrate-binding pocket in the absence of bound substrate or co-factors. Therefore, although these enzymes likely employ the same catalytic mechanism, the substrate- and flavin co-enzyme-binding mechanisms appear to differ significantly. Both of the active sites in the *Actinomadura kijaniata* sugar N-oxygenase and the *Acinetobacter baumannii* monooxygenase exhibit tunnel-like channels that are open to solvent

on both sides, and the hydrophilic substrates and flavins for these enzymes might access the catalytic site through specific gates located at the two entrances. However, in DszC, the active site is a pocket with a hydrophobic base and a solvent-exposed opening; therefore, the hydrophobic substrate DBT and the flavin co-enzyme might only reach the internal space of the pocket through this single entrance.

DszC is a flavin-dependent DBT monooxygenase; therefore, it must interact with both the substrate and a flavin co-enzyme. On the basis of the structure of the substrate-binding pocket, we hypothesize that the two chambers may serve as separate containers for the substrate and co-enzyme. The inner chamber is small and hydrophobic and facilitates binding of the DBT substrate, whereas our observations suggest that the outer chamber is sufficiently large for the triple-ring head of FMN to access [Fig. 3(B,C)]. In addition, the positive charge on the opening of the substrate-binding pocket could stabilize the FMN phosphate-group tail. Furthermore, as this opening is relatively narrow, it may need to undergo specific conformational changes to facilitate entry of the FMN triple-ring head. The polar groups between the inner and outer chambers may facilitate electron transfer between DBT and the co-enzyme.

Recently, the structure of a closely related homotetrameric DszC homolog has been reported.[39] A comparison of this structure with the present DszC structure indicates that the overall structures are nearly identical except that two distinct conformations in the loops adjacent to the entrance of the substrate-binding pocket (residues 280-295, between α9 and α10) were observed in the DszC homolog structure. On the basis of these features, Liu *et al.* defined an "open" and a "closed" state for DszC and hypothesized that these two states may correspond to the free and ligand-bound DszC. Unfortunately, we did not observe this conformational distinction in the present DszC structure; all monomers in our structure represent the "closed" state. However, consistent with the observation of these authors, we also observed that the entrance of each substrate-binding pocket is narrow and composed of two neighboring chains (e.g., chains A and D), which suggests that the entrance of the substrate-binding pocket may undergo conformational change to allow substrate access, as previously described. We strongly support the hypothesis proposed by these authors in this regard. In addition to these similarities, we found significant differences in the binding position of the DBT substrate. Based on the structural comparison between DszC and the monooxygenase from *Acinetobacter baumannii* in complex with its substrate and coenzyme [Fig. 3(C)], as well as the results of the activity assay of the C-terminal and F250 mutants, we propose that the inner chamber of the substrate-binding pocket may represent the site for DBT binding, as previously described. In contrast, the docked DBT molecule in the structure reported by Liu *et al.* is located at an entirely different position [the approximate position is indicated by an asterisk in Fig. 3(A,B)]. In light of this clear difference, we believe it remains premature to definitively identify the DBT-binding site or propose a detailed catalytic mechanism for DszC prior to the determination of a DszC-FMN-DBT complex structure.

The monooxygenase from *Mycobacterium tuberculosis* can form either a tetramer or an octamer, and conformational changes in the C-terminus may accompany these shifts in oligomerization state.[12] In DszC, although the C-terminus also appears to be linked with the oligomerization state of the enzyme—suggesting that truncating the tail would impair tetramerization—conformational changes similar to what is observed in *Mycobacterium tuberculosis* monooxygenase were not observed in the DszC C-terminus. Moreover, DszC only formed tetramers in solution, as previously described, which suggests that DszC cannot undergo an oligomerization shift or form octamers, as has been demonstrated for the monooxygenase from *mycobacterium tuberculosis*.

Homologous proteins with similar tetrameric structures, such as the amino sugar-oxidizing enzyme from *Micromonospora carbonacea* var. *Africana*,[40] the human isovaleryl-CoA dehydrogenase[41] and the rat short-chain acyl-CoA dehydrogenase,[42] naturally lack the C-terminal tails beyond the last helices (Supporting Information Fig. S3). However, the DszC C-terminus is closely involved in tetramerization, which suggests that DszC may have certain alternative mechanisms to direct participation at the interaction interface. As previously mentioned, α12 contributes greater than one-third of the buried surface area per subunit, and displacement of this helix may seriously affect interactions between subunits. Notably, in comparison to the homologous proteins, α12 in DszC is located at a greater distance from the core structure of the enzyme (Supporting Information Fig. S2). We speculate that the C-terminus may contribute to this unique characteristic of DszC by pushing the helix outward and maintaining proper helix positioning. In other words, without the C-terminus, the α12 helix may become localized further inward and become detached from the tetramerization interface, thus impairing tetramerization. Moreover, without the C-terminus, helix α12 may adopt certain unpredictable conformations and impede tetramerization. On the other hand, the R338A or C-terminus truncation mutations disrupted the polar interaction between the 338-Arg side chain on α10 and the 417-Ser main-chain carboxyl group. As a consequence, upon losing this interaction with 338-Arg, helix α10, which also plays an important role in tetramerization, may undergo certain conformational changes and impair tetramer stability.

ACKNOWLEDGMENTS

The authors thank Zheng Wang for performing the analytical ultracentrifugation analysis.

REFERENCES

1. Torktaz I, Etemadifar Z, Derikvand P. Comparative modeling of DszC, an enzyme in biodesulfurization, and performing in silico point mutation for increasing tendency to oil. Bioinformation 2012; 8:246–250.
2. Aggarwal S, Karimi IA, Kilbane Ii JJ, Lee DY. Roles of sulfite oxidoreductase and sulfite reductase in improving desulfurization by *Rhodococcus erythropolis*. Mol BioSystems 2012;8:2724–2732.
3. Kabe T, Ishihara A, Tajima H. Hydrodesulfurization of sulfur-containing polyaromatic compounds in light oil. Ind Eng Chem Res 1992;31:1577–1580.
4. Piddington CS, Kovacevich BR, Rambosek J. Sequence and molecular characterization of a DNA region encoding the dibenzothiophene desulfurization operon of Rhodococcus sp. strain IGTS8. Appl Environ Microbiol 1995;61:468–475.
5. Calzada J, Zamarro MT, Alcon A, Santos VE, Diaz E, Garcia JL, Garcia-Ochoa F. Analysis of dibenzothiophene desulfurization in a recombinant *Pseudomonas putida* strain. Appl Environ Microbiol 2009;75:875–877.
6. Olmo CHd, Santos VE, Alcon A, Garcia-Ochoa F. Production of a *Rhodococcus erythropolis* IGTS8 biocatalyst for DBT biodesulfurization: influence of operational conditions. Biochem Eng J 2005;22: 229–237.
7. Denome SA, Oldfield C, Nash LJ, Young KD. Characterization of the desulfurization genes from Rhodococcus sp. strain IGTS8. J Bacteriol 1994;176:6707–6716.
8. Gray KA, Pogrebinsky OS, Mrachko GT, Xi L, Monticello DJ, Squires CH. Molecular mechanisms of biocatalytic desulfurization of fossil fuels. Nat Biotechnol 1996;14:1705–1709.
9. Gupta N, Roychoudhury PK, Deb JK. Biotechnology of desulfurization of diesel: prospects and challenges. Appl Microbiol Biotechnol 2005;66:356–366.
10. Kilbane JJ, II. Microbial biocatalyst developments to upgrade fossil fuels. Curr Opin Biotechnol 2006;17:305–314.
11. Ohshiro T, Ohkita R, Takikawa T, Manabe M, Lee WC, Tanokura M, Izumi Y. Improvement of 2′-hydroxybiphenyl-2-sulfinate desulfinase, an enzyme involved in the dibenzothiophene desulfurization pathway, from *Rhodococcus erythropolis* KA2-5-1 by site-directed mutagenesis. Biosci Biotechnol Biochem 2007;71:2815–2821.
12. Thoden JB, Branch MC, Zimmer AL, Bruender NA, Holden HM. Active site architecture of a sugar N-oxygenase. Biochemistry 2013; 52:3191–3193.
13. Bruender NA, Thoden JB, Holden HM. X-ray structure of kijd3, a key enzyme involved in the biosynthesis of D-kijanose. Biochemistry 2010;49:3517–3524.
14. Dresen C, Lin LY, D'Angelo I, Tocheva EI, Strynadka N, Eltis LD. A flavin-dependent monooxygenase from *Mycobacterium tuberculosis* involved in cholesterol catabolism. J Biol Chem 2010;285:22264–22275.
15. Duan X, Zhang L, Zhou D, Ji K, Ma T, Shui W, Li G, Li X. Crystallization and preliminary structural analysis of dibenzothiophene monooxygenase (DszC) from *Rhodococcus erythropolis*. Acta Crystallogr Sect F Struct Biol Crystallization Commun 2013;69 (Part 6): 597–601.
16. Kabsch W. Xds. Acta Crystallogr Sect D Biol Crystallogr 2010;66 (Part 2):125–132.
17. Otwinowski Z, Minor W. Processing of X-ray diffraction data collected in oscillation mode. In: Carter CW, Jr., Sweet RM, editors. Methods in enzymology: macromolecular crystallography (part A), Vol. 276. New York: Academic Press; 1997. pp 307–326.
18. Winn MD, Ballard CC, Cowtan KD, Dodson EJ, Emsley P, Evans PR, Keegan RM, Krissinel EB, Leslie AG, McCoy A, McNicholas SJ, Murshudov GN, Pannu NS, Potterton EA, Powell HR, Read RJ, Vagin A, Wilson KS. Overview of the CCP4 suite and current developments. Acta Crystallogr Sect D Biol Crystallogr 2011;67 (Part 4): 235–242.
19. McCoy AJ, Grosse-Kunstleve RW, Adams PD, Winn MD, Storoni LC, Read RJ. Phaser crystallographic software. J Appl Crystallogr 2007;40 (Part 4):658–674.
20. Murshudov GN, Skubak P, Lebedev AA, Pannu NS, Steiner RA, Nicholls RA, Winn MD, Long F, Vagin AA. REFMAC5 for the refinement of macromolecular crystal structures. Acta Crystallogr Sect D Biol Crystallogr 2011;67 (Part 4):355–367.
21. Adams PD, Afonine PV, Bunkoczi G, Chen VB, Davis IW, Echols N, Headd JJ, Hung LW, Kapral GJ, Grosse-Kunstleve RW, McCoy AJ, Moriarty NW, Oeffner R, Read RJ, Richardson DC, Richardson JS, Terwilliger TC, Zwart PH. PHENIX: a comprehensive Python-based system for macromolecular structure solution. Acta Crystallogr Sect D Biol Crystallogr 2010;66 (Part 2):213–221.
22. Emsley P, Lohkamp B, Scott WG, Cowtan K. Features and development of Coot. Acta Crystallogr Sect D Biol Crystallogr 2010;66 (Part 4):486–501.
23. Davis IW, Murray LW, Richardson JS, Richardson DC. MOLPROBITY: Structure validation and all-atom contact analysis for nucleic acids and their complexes. Nucleic Acids Res 2004;32(Web Server issue):W615–W619.
24. DeLano WL. The PyMOL Molecular graphics system. San Carlos, CA: DeLano Scientific; 2002.
25. Ho SN, Hunt HD, Horton RM, Pullen JK, Pease LR. Site-directed mutagenesis by overlap extension using the polymerase chain reaction. Gene 1989;77:51–59.
26. Zhang L, Chen R, Dong Z, Li X. Overexpression, crystallization and preliminary X-ray crystallographic analysis of the phosphotriesterase from *Mycobacterium tuberculosis*. Acta Crystallogr Sect F Struct Biol Crystallization Commun 2013;69 (Part 1):57–60.
27. Schuck P. On the analysis of protein self-association by sedimentation velocity analytical ultracentrifugation. Anal Biochem 2003;320: 104–124.
28. Schuck P. Size-distribution analysis of macromolecules by sedimentation velocity ultracentrifugation and lamm equation modeling. Biophys J 2000;78:1606–1619.
29. Li GQ, Ma T, Li SS, Li H, Liang FL, Liu RL. Improvement of dibenzothiophene desulfurization activity by removing the gene overlap in the dsz operon. Biosci Biotechnol Biochem 2007;71:849–854.
30. Watanabe K, Noda K, Konishi J, Maruhashi K. Desulfurization of 2,4,6,8-tetraethyl dibenzothiophene by recombinant Mycobacterium sp. strain MR65. Biotechnol Lett 2003;25:1451–1456.
31. Li GQ, Li SS, Zhang ML, Wang J, Zhu L, Liang FL, Liu RL, Ma T. Genetic rearrangement strategy for optimizing the dibenzothiophene biodesulfurization pathway in *Rhodococcus erythropolis*. Appl Environ Microbiol 2008;74:971–976.
32. Ohshiro T, Kojima T, Torii K, Kawasoe H, Izumi Y. Purification and characterization of dibenzothiophene (DBT) sulfone monooxygenase, an enzyme involved in DBT desulfurization, from *Rhodococcus erythropolis* D-1. J Biosci Bioeng 1999;88:610–616.
33. Matsubara T, Ohshiro T, Nishina Y, Izumi Y. Purification, characterization, and overexpression of flavin reductase involved in dibenzothiophene desulfurization by *Rhodococcus erythropolis* D-1. Appl Environ Microbiol 2001;67:1179–1184.
34. Ohshiro T, Ishii Y, Matsubara T, Ueda K, Izumi Y, Kino K, Kirimura K. Dibenzothiophene desulfurizing enzymes from moderately thermophilic bacterium *Bacillus subtilis* WU-S2B: purification, characterization and overexpression. J Biosci Bioeng 2005;100:266–273.
35. Larkin MA, Blackshields G, Brown NP, Chenna R, McGettigan PA, McWilliam H, Valentin F, Wallace IM, Wilm A, Lopez R, Thompson JD, Gibson TJ, Higgins DG. Clustal W and Clustal X version 2.0. Bioinformatics 2007;23:2947–2948.
36. Goujon M, McWilliam H, Li W, Valentin F, Squizzato S, Paern J, Lopez R. A new bioinformatics analysis tools framework at EMBL-EBI. Nucleic Acids Res 2010;38:W695–W699.
37. Alfieri A, Fersini F, Ruangchan N, Prongjit M, Chaiyen P, Mattevi A. Structure of the monooxygenase component of a two-component

flavoprotein monooxygenase. Proc Natl Acad Sci USA 2007;104: 1177–1182.
38. Orville AM, Lountos GT, Finnegan S, Gadda G, Prabhakar R. Crystallographic, spectroscopic, and computational analysis of a flavin C4a-oxygen adduct in choline oxidase. Biochemistry 2009;48:720–728.
39. Liu S, Zhang C, Su T, Wei T, Zhu D, Wang K, Huang Y, Dong Y, Yin K, Xu S, Xu P, Gu L. Crystal structure of DszC from Rhodococcus sp. XP at 1.79 A. Proteins 2014. DOI: 10.1002/prot.24525.
40. Vey JL, Al-Mestarihi A, Hu Y, Funk MA, Bachmann BO, Iverson TM. Structure and mechanism of ORF36, an amino sugar oxidizing enzyme in everninomicin biosynthesis. Biochemistry 2010;49:9306–9317.
41. Tiffany KA, Roberts DL, Wang M, Paschke R, Mohsen AW, Vockley J, Kim JJ. Structure of human isovaleryl-CoA dehydrogenase at 2.6 A resolution: structural basis for substrate specificity. Biochemistry 1997;36:8455–8464.
42. Battaile KP, Molin-Case J, Paschke R, Wang M, Bennett D, Vockley J, Kim JJ. Crystal structure of rat short chain acyl-CoA dehydrogenase complexed with acetoacetyl-CoA: comparison with other acyl-CoA dehydrogenases. J Biol Chem 2002;277:12200–12207.